Misfit dislocations of anisotropic magnetoresistant Nd$_{0.45}$Sr$_{0.55}$MnO$_3$ thin films grown on SrTiO$_3$ (110) substrates

Y.L. Tang, Y.L. Zhu [*], H. Meng, Y.Q. Zhang, X.L. Ma

Shenyang National Laboratory for Materials Science, Institute of Metal Research, Chinese Academy of Sciences, Shenyang 110016, People's Republic of China

Abstract

Nd$_{0.45}$Sr$_{0.55}$MnO$_3$ is an A-type antiferromagnetic manganite showing obvious angular-dependent magnetoresistance, which can be tuned by misfit strain. The misfit strain relaxation of Nd$_{0.45}$Sr$_{0.55}$MnO$_3$ thin films is of both fundamental and technical importance. In this paper, microstructures of epitaxial Nd$_{0.45}$Sr$_{0.55}$MnO$_3$ thin films grown on SrTiO$_3$ (110) substrates by pulsed laser deposition were investigated by means of (scanning) transmission electron microscopy. The Nd$_{0.45}$Sr$_{0.55}$MnO$_3$ thin films exhibit a two-layered structure: a continuous perovskite layer epitaxial grown on the substrate followed by epitaxially grown columnar nanostructures. An approximately periodic array of misfit dislocations is found along the interface with line directions of both $\langle 111 \rangle$ and $[001]$. High-resolution (scanning) transmission electron microscopy reveals that all the misfit dislocations possess $a\langle 110 \rangle$-type Burgers vectors. A formation mechanism based on gliding or climbing of the dislocations is proposed to elucidate this novel misfit dislocation configuration. These misfit dislocations have complex effects on the strain relaxation and microstructure of the films, and thus their influence needs further consideration for heteroepitaxial perovskite thin film systems, especially for films grown on substrates with low-symmetry surfaces such as SrTiO$_3$ (110) and (111), which are attracting attention for their potentially new functions.
© 2012 Acta Materialia Inc. Published by Elsevier Ltd. All rights reserved.

Keywords: High resolution (scanning) transmission electron microscopy; Misfit dislocations; Perovskite oxides; Misfit relaxation

1. Introduction

Colossal magnetoresistive (CMR) manganites Re$_{1-x}$A$_x$MnO$_3$ (Re, rare-earth ion; A, alkaline-earth ion) are perovskite polymorph oxides which have been well studied in the quest for a fundamental understanding of their physical properties such as magnetotransport behaviors, phase and magnetic transformations and for their potential applications [1–7]. Among these compounds, Nd$_{0.45}$Sr$_{0.55}$MnO$_3$ is a typical metallic A-type antiferromagnetic (AFM) manganite that exhibits a uniform alignment of the d$x^2 - y^2$-type orbital, which has been recognized to control transport properties in the metallic phase [8–10]. In addition, it was found that, in contrast to the common Re$_{1-x}$A$_x$MnO$_3$ compounds in which, with decreasing temperature, a paramagnetic PM (or AFM) to ferromagnetic (FM) transition takes place accompanied by an insulator–metal transition, in Nd$_{0.45}$Sr$_{0.55}$MnO$_3$, a PM to AFM transition occurs at the Néel temperature (T$_N$), and simultaneously there is a changes from an insulator to a metallic phase below T$_N$ until 80 K, then to an insulator again [8,10]. In the past few years, robust investigations have been performed in an attempt to reveal the underlying correlations between the magnetic and crystal structures and the transport properties [8,9,11].

Thin film engineering is commonly used to introduce misfit strains into functional perovskite oxides which can tune their performance because of lattice mismatch and the difference in thermal expansion coefficients between film and substrate. This is particularly true for manganite perovskite oxides, whose electrical and magnetic properties as well as

---

* Corresponding author. Tel.: +86 24 83978629; fax: +86 24 23971215.
E-mail address: ylzhu@imr.ac.cn (Y.L. Zhu).

their structures are inherently sensitive to the misfit strains. It has been found that when $Re_{1-x}A_xMnO_3$ compounds are grown on perovskite substrates as epitaxial thin films, the lattice mismatch between the film and substrate introduces a two-dimensional strain in the films. Moreover, the chemical constituents [12], crystal structures [13] and physical properties [14,15] of the films are dramatically dependent on the two-dimensional strain. Taking $Nd_{0.45}Sr_{0.55}MnO_3$ film grown on $SrTiO_3$ (0 0 1) with 6 nm thickness as an example, the bulk value T_N changed from 225 to 282 K. Moreover, both 2-fold and 4-fold symmetric angular-dependent magnetoresistance (AMR) are observed in this film, which is remarkably different from previous studies [11].

On the other hand, for perovskite-based heteroepitaxial systems, the misfit strains are generally accommodated by misfit dislocations (MDs) when the film thickness exceeds a critical value [16,17]. The process of MD nucleation and multiplication is strongly dependent on the dislocation behavior of the films or substrates themselves [17–19]. As a common substrate material for perovskite thin film growth, $SrTiO_3$ has been extensively studied in order to understand its dislocation behavior, provide an analogue for the dislocation behaviors of perovskite oxides [20–23]. An interesting result is that the $a\langle 110 \rangle$-type dislocations in $SrTiO_3$ are mainly responsible for the dislocation gliding over a wide temperature range. These studies are crucial for understanding the MD behavior in perovskite thin films. Commonly, MDs in these epitaxial systems have Burgers vectors of $a\langle 100 \rangle$-type with line directions of $\langle 100 \rangle$, originating from dislocation reaction [17]; $a\langle 110 \rangle$-type with line directions of $\langle 100 \rangle$, originating from perfect dislocation glide in perovskite oxides [17,20,24]; and $1/2a\langle 110 \rangle$-type with line directions of $\langle 100 \rangle$, accompanied by an antiphase boundary [17,25,26]. The existence of these MDs will relax the strains in films and thus affects their properties; therefore it is essential to elucidate MD behavior in these systems.

Moreover, it has been reported recently that the substrate surface—e.g. using $SrTiO_3$ (1 1 0) rather than the more common $SrTiO_3$ (0 0 1)—also influences the physical properties of $Nd_{1-x}Sr_xMnO_3$-based thin films. By using (1 1 0) substrates, bulk-like behaviors were observed in $Nd_{0.5}Sr_{0.5}MnO_3$ films [2,27], whereas for films grown on $SrTiO_3$ (0 0 1), a clear metal–insulator transition has not been observed [27,28]. Unique filamentary metallic domains were found aligning preferentially along certain crystal axes of $SrTiO_3$ (1 1 0) substrate for the $Nd_{0.5}Sr_{0.5}MnO_3/SrTiO_3$ (1 1 0) [2]. A new type of orbital ordering was also observed in this film, which exhibits a clear first-order transition [29]. These results suggest that the anisotropic $SrTiO_3$ (1 1 0) substrate offers a new means to modulate the properties of manganite films, which may enable us to finely tune the Jahn–Teller distortion and thereby manipulate the metal–insulator transition [14]. Nevertheless, the detailed strain relaxation behavior of $Nd_{1-x}Sr_xMnO_3/SrTiO_3$ (1 1 0) systems and the possible interface defects remain enigmatic.

Since information on the strain, structure and microstructure of these oxide materials is of great importance

for understanding the interplay of structure, magnetism and electronic transport, it is necessary to investigate these properties in detail. (Scanning) transmission electron microscopy ((S)TEM), which can provide a direct local interpretation of chemical, structural and even electronic information of the interface on atomic scale, is a very powerful tool to investigate interfacial structures, especially for studying the strain and defects in thin films and their interfaces [30–32]. In contrast, although much attention has been paid to the physical properties of both the bulk and thin-film form of $Nd_{0.45}Sr_{0.55}MnO_3$ [8–11], the misfit relaxation and the possible MD configuration in $Nd_{0.45}Sr_{0.55}MnO_3$ thin films are still not clear, especially in films prepared on the anisotropic and promisingly function tunable substrate $SrTiO_3$ (1 1 0).

In this paper, we report on a detailed study of MD structures of $Nd_{0.45}Sr_{0.55}MnO_3$ thin films grown epitaxially on $SrTiO_3$ (1 1 0) by the pulsed laser deposition (PLD) technique. MDs with Burgers vectors $a\langle 110 \rangle$ and line directions of both [0 0 1] and $\langle 111 \rangle$ were observed along the interface, which constitute the major interfacial defects in these films. The formation mechanism of these MDs is proposed and discussed.

2. Experimental

Epitaxial $Nd_{0.45}Sr_{0.55}MnO_3$ (NSMO) films were grown on $SrTiO_3$ (1 1 0) (STO (1 1 0)) substrates by PLD (550 mJ, 2 Hz). Before deposition, the substrate was heated at 750 °C for 20 min to clean the substrate surface and the laser was focused on a ceramic $Nd_{0.45}Sr_{0.55}MnO_3$ target for 30 min presputtering to clean the target surface. Throughout the deposition process, an oxygen pressure of 40 Pa was maintained. After deposition, the film was annealed at 750 °C in an oxygen pressure of 2×10^4 Pa for 10 min, and then cooled to room temperature at a cooling rate of 5 °C min^{-1}. For comparison, NSMO films with the same composition were prepared on STO (0 0 1) under the same deposition conditions.

The specimens for cross-sectional observations were prepared by slicing, gluing, grinding, dimpling, and finally ion-milling. A Gatan 656 Dimple Grinder was used for dimpling. Ar-ion-milling was performed by using a Gatan 691 PIPS. During the ion-milling, an accelerating voltage of 5 kV and an incident angle of 7° were used first, and then an accelerating voltage of 2.5 kV and an incident angle of 3–4° were selected for the final cleaning. Plan-view TEM samples were thinned and ion-milled only from the STO substrate side until the Ar ion beam perforated the samples. A Tecnai G^2 F30 transmission electron microscope working at 300 kV, equipped with a high-angle-annular-dark-field (HAADF) detector, energy-dispersive X-ray spectroscopy (EDS) systems and a post-column Gatan imaging-filter, was used for diffraction contrast analysis, high-resolution transmission electron microscopy (HRTEM) imaging and high-resolution (HR) STEM imaging. The point resolutions of the TEM are 0.20 and 0.17 nm for TEM and STEM model, respectively.

3. Results

3.1. General information

At room temperature, the NSMO crystal has a body-centered tetragonal structure which belongs to the I4/mcm space group with lattice parameters of a = b = 0.5390 nm and c = 0.7778 nm [3]. If room temperature NSMO is treated as a slightly distorted pseudocubic structure, then the average lattice parameter should be a = 0.3837 nm. In order to consider epitaxy, it is equally important to compare the corresponding interplanar distance rather than the interatomic distances, i.e. the lattice parameters. The STO (110) surface has two different in-plane orthogonal crystal axes: [001] and [1$\bar{1}$0]; the corresponding lattice mismatches lie in between the planes of STO (001) and NSMO (001), STO (1$\bar{1}$0) and NSMO (1$\bar{1}$0), which is different from the commonly used STO (001). In the cubic STO substrate, $d_{100} = d_{010} = d_{001} = 0.3905$ nm, and $d_{110} = 0.2761$ nm. The corresponding interplanar distances in the NSMO bulk are $d_{100} = 0.3837$ nm and $d_{110} = 0.2713$ nm. It is thus determined that the films are under tensile stress in the present films. In this paper, the NSMO crystal is treated as a pseudocubic structure for simplicity.

3.2. (Scanning) transmission electron microscopy

TEM investigations indicate that the interfacial structure of the NSMO/STO (110) systems is complicated. Fig. 1a is a cross-sectional bright-field image taken with the incident electron beam along the [$\bar{1}$10] zone axis of STO showing the morphology of the NSMO/STO (110) systems. The film is about 200 nm thick. It is noted that the film exhibits a two-layered structure: a continuous layer 30 nm thick which is directly grown on the substrate, and a columnar layer which is grown from the continuous layer. No obvious defects can be observed along the interface under this imaging condition. However, when we used other diffraction vectors to construct the images, the contrast of the film as well as of the interface changes dramatically. Fig. 1b is a weak-beam, dark-field (WBDF) image of the NSMO/STO (110) films viewed near the [001] zone axis of STO with g = 1$\bar{1}$0 under the (g, 4g) condition. From this image, it is observed that a high density of interfacial defects accumulated at the interface, consisting of two groups of interfacial dislocations with different line directions, denoted by arrows. It should be noted that these two groups of dislocations are not parallel to each other. Fig. 1c is a cross-sectional WBDF TEM image of the NSMO/STO (110) viewed near the [$\bar{1}$1$\bar{1}$] zone axis of STO with g = 10$\bar{1}$ under the (g, 4g) condition. The contrast of two groups of dislocations is still visible but changes slightly as indicated by arrows. In order to exactly identify the line directions of these dislocations, plan-view observations are necessary. Tilting experiments in conventional TEM revealed some characteristics of the dislocations. Fig. 2 is a plan-view low-magnification TEM image of
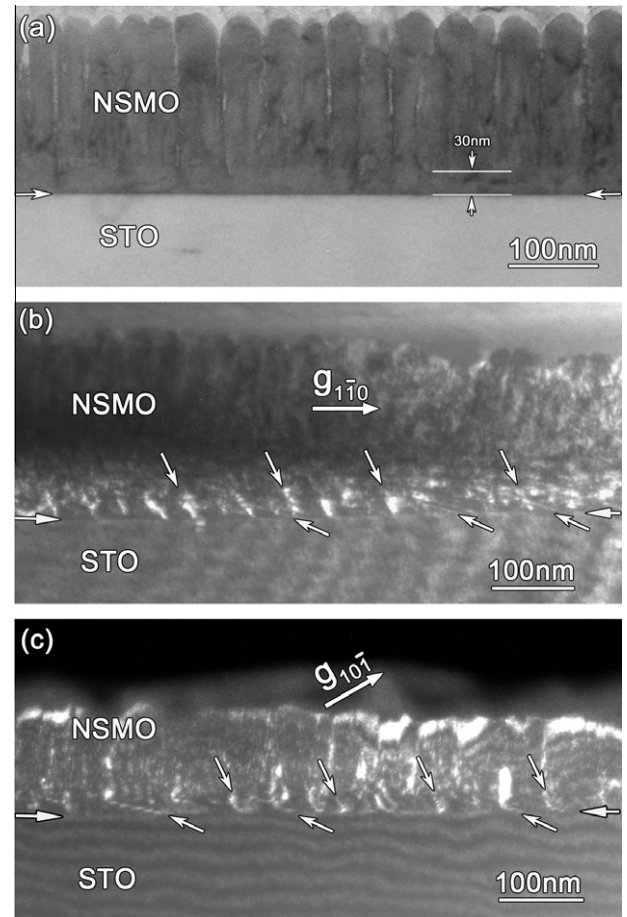

Fig. 1. (a) Cross-sectional bright-field image of NSMO/STO (110) heteroepitaxy showing the morphology of the films. The film exhibits a two-layered structure. No defects can be clearly observed along the interface. (b and c) Cross-sectional WBDF images taken with g = (1$\bar{1}$0) and g = (10$\bar{1}$) under (g, 4g) conditions, respectively. Under these imaging conditions, two groups of MDs with different line directions are observed along the interfaces and are indicated by arrows.

the NSMO/STO (110) system taken from an area that includes both the film and substrate. This image was recorded by tilting the plan-view sample ∼25–30° away from the [110] zone axis of STO. Three sets of dislocation lines along the [001], [$\bar{1}$1$\bar{1}$] and [$\bar{1}$11] directions of STO can be observed, as indicated by arrows. The asymmetric distribution of the lines along the two ⟨111⟩ directions may be attributed to an inhomogeneous distribution of interface strain. However, this imaging condition gives a subtle artifact related to the 2-D image–3-D specimen relationship in a TEM: due to the large tilt angle away from the [110] zone axis of STO, the projected angles between the two ⟨111⟩ MDs change from the true values of 71° to 61°. As expected, the angle between [$\bar{1}$1$\bar{1}$] and [$\bar{1}$11] in the cubic STO crystal is calculated to be 70.5°. However, the angle between [$\bar{1}$1$\bar{1}$] and [$\bar{1}$11] MDs in Fig. 2 is about 61°. To reveal the angle more precisely, the plan-view sample must be oriented very close to the [110] zone axis of STO. The inset is a low-magnification, dark-field image showing the true angle between [$\bar{1}$1$\bar{1}$] and [$\bar{1}$11] MDs. This
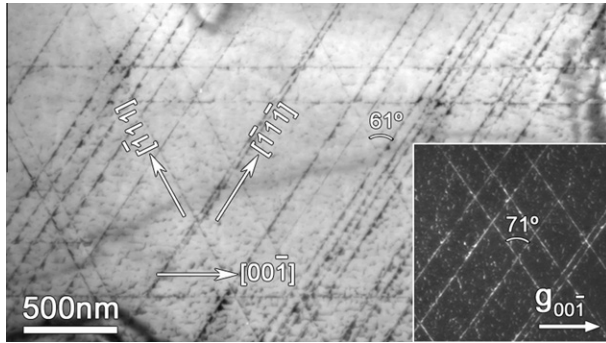
Fig. 2. Plan-view low-magnification TEM image of the NSMO/STO (110) system viewed a few tens of degrees away from the [110] zone axis of STO. Three sets of dislocation lines with the directions along the [001], [$\bar{1}1\bar{1}$] and [$\bar{1}11$] directions of STO were observed. The inset is a dark-field TEM image viewed very close to the [110] zone axis of STO taken with g = (00$\bar{1}$). The contrast of dislocations with [001] line directions is lost.
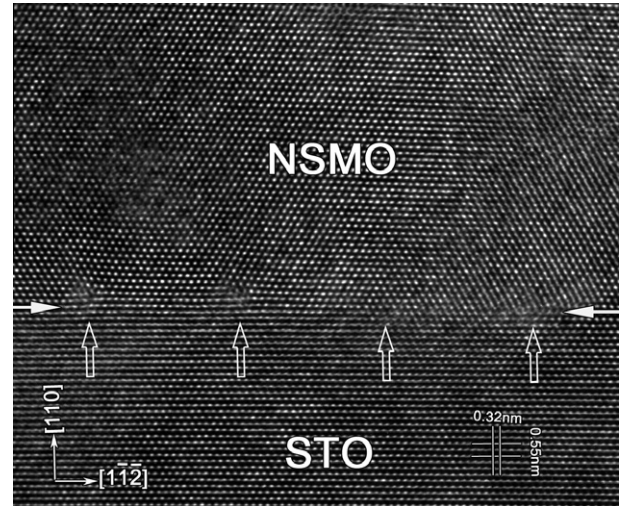

Fig. 3. Low-magnification cross-sectional HRTEM image of the NSMO/STO (110) heteroepitaxy. Vertical arrows denote the positions of interfacial dislocations.

image was taken just a few degrees away from the [110] zone axis of STO with g = (00$\bar{1}$). The angle is measured to be about 71°, which is more consistent with the angle (70.5°) between [$\bar{1}1\bar{1}$] and [$\bar{1}11$] STO. Simultaneously, however, we lose the contrast of [001] MDs because of the specific two-beam condition.

This kind of MD configuration is very different from the ones in previous studies on [001]-oriented thin-film systems [17,24], where MDs with Burgers vectors of both b = $a\langle 100 \rangle$ and b = $a\langle 110 \rangle$ type form a rectangular network with line directions of $\langle 100 \rangle$. The MD configuration in the present study is very complex and it is difficult to determine the Burgers vectors of the dislocations simply by diffraction contrast analysis. Nevertheless, plan-view, low-magnification TEM imaging is a straightforward way to identify the dislocation line directions and facilitates the identification of the characters of dislocations [19]. To identify the characters of the MDs, HR(S)TEM imaging was performed. Fig. 3 is a low-magnification cross-sectional HRTEM image taken along the [$\bar{1}1\bar{1}$] direction of STO showing the interface of the NSMO/STO (110) film. An array of misfit dislocations is found nearly periodically distributed along the interface, and the position of each misfit dislocation is denoted by the vertical arrows. The dislocation are spaced about 7 nm apart. One of these dislocations is shown at a larger magnification in Fig. 4a to display the structural details. Fig. 4a is a HRSTEM image that also provides composition information. The slightly dark contrast around the dislocation core implies that cation deficiency may exist at the core area. From Fig. 4a, it is noted that the MD core looks sharp and no blurred effect due to the non-edge-on dislocation was observed [33]. This kind of MD configuration indicates that this dislocation may possess a component with [$\bar{1}1\bar{1}$] line direction, and was imaged in an edge-on condition. By drawing a Burgers circuit surrounding the dislocation core, the Burgers vector b is determined as 1/3a[21$\bar{1}$]. Because b = 1/3a[21$\bar{1}$] is not a translation vector in perovskite oxides, it is probably a

projected component of a perfect Burgers vector. Since no other defects are found to accompany the MD, the perfect Burgers vector must show a projected component when imaged along the edge-on direction, i.e. the MD line direction. This consideration leads to possible Burger vectors of either a[01$\bar{1}$] or a[100]—both are translation vectors in perovskite thin films, as illustrated at the schematic diagrams in the lower part of Fig. 4a: left, a[01$\bar{1}$] and a[100] are overlapped in the projected unit cell model (indicated by arrow) viewed along [$\bar{1}1\bar{1}$] direction of STO; right, a[01$\bar{1}$] and a[100] are distinguished in the stereogram unit cell model (indicated by arrows). To determine the Burgers vector accurately, it is essential to observe the dislocation configuration from other directions because the two possible Burger vectors mentioned above will give different projected components from other specific directions. For the [$\bar{1}10$] zone axis, the vector a[01$\bar{1}$] will give a projected component b = 1/2a[11$\bar{2}$], while a[100] will give a projected component b = 1/2a[110]. To verify this assumption, we tilted the sample and took the image from the single dislocation of Fig. 4a along the [$\bar{1}10$] direction of STO. In Fig. 4b, the dislocation core is blurred due to the non-edge-on effect [33], i.e. the dislocation line is now inclined to the electron beam. By drawing a Burgers closure, the Burgers vector is determined to be 1/2a[11$\bar{2}$], which means that the dislocations in the present study have a perfect Burgers vector of b = a[01$\bar{1}$]. The bottom schematic diagram of Fig. 4b, in which only one perfect Burgers vector is identified, supports this conclusion. This b = $a\langle 110 \rangle$-type MD is very common in perovskite film systems [24,34], the MDs with line directions of $\langle 111 \rangle$ have not yet been reported. Furthermore, it is reasonable to deduce that MDs with other $\langle 111 \rangle$ line directions may exist in the present films because the $\langle 111 \rangle$ of cubic STO are crystallographically equivalent. For the dislocations with line direction of [001], it is reasonable to image them along the [001] direction of STO. Fig. 5 is an HRSTEM image of
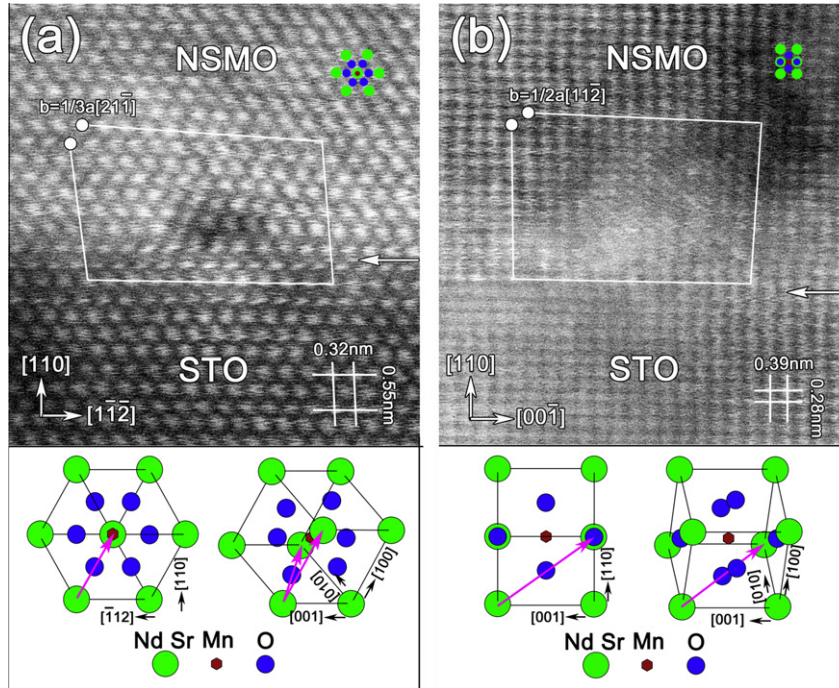
Fig. 4. (a) HRSTEM image of a MD viewed along the $[\bar{1}1\bar{1}]$ direction of STO. (b) The same MD as in (a) viewed along the $[\bar{1}10]$ zone axis. The bottom schematic diagrams illustrate the possible Burgers vectors. Combining (a) with (b), only Burgers vector b = $a[01\bar{1}]$ is possible.

a dislocation viewed along the [001] of STO. The dislocation core appears blurred due to the strong lattice distortion [33]. The interface is coherent with no other planar defects. By drawing a Burgers closure, Burgers vector b = $a[1\bar{1}0]$ was identified. Based on the TEM observations, the possible projected Burgers vectors, line directions and perfect Burgers vectors for the MDs in the NSMO/STO (110) film are summarized in Table 1. As indicated by asterisks in Table 1, dislocations with projected Burgers vector b = $1/3a[\bar{1}\bar{2}\bar{1}]$ were not directly observed in our experiments. However, due to the crystallographically equivalent factors, the b = $a[\bar{1}0\bar{1}]$ MDs should be available.

4. Discussion

The MDs in NSMO/STO (110) thin film were identified to have Burgers vector $a\langle110\rangle$ and line directions of both $\langle111\rangle$ and [001]. These characteristics are quite different from previous studies, and how the misfit strains were released by the formation of these MDs and what effects they have on the microstructure of NSMO film as well as the formation mechanism of these dislocations should be elucidated.

4.1. The misfit strain relaxation behaviors and the corresponding effects on the microstructure

Because the dislocations observed in the present study have two different characters, the misfit strain relaxation in the present thin-film system will be understood from
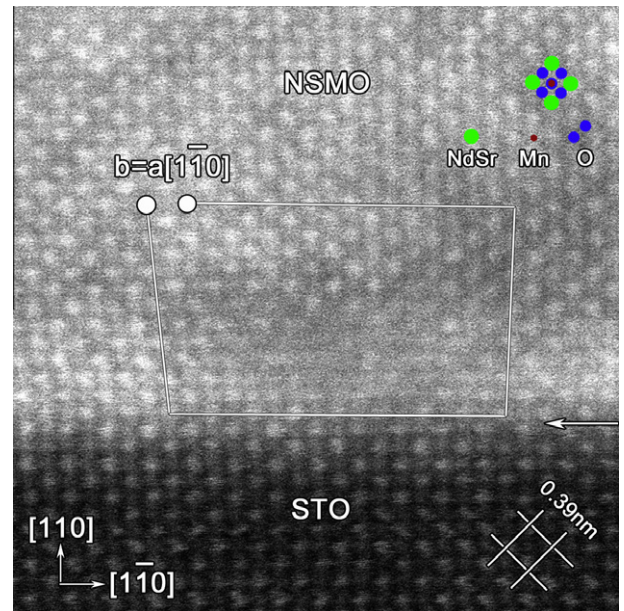

Fig. 5. HRSTEM image viewed along [001] direction of STO. The Burgers vector is determined as $a[1\bar{1}0]$. The interface is marked with a horizontal arrow. A projected pseudocubic unit cell model of NSMO is given at top right to match the image.

two aspects. First we discuss the contributions from the dislocations with Burgers vector $a\langle011\rangle$ (b = $\langle uvw\rangle$ where $w \neq 0$) and line directions of $\langle111\rangle$. Due to the specific substrate surface, the Burgers vectors for the observed dislocations are projected components of perfect dislocations. Therefore, it is reasonable to decompose the perfect one

Table 1
All possible projected Burgers vectors and perfect Burgers vectors for the MDs in NSMO/STO (1 1 0).

MD line direction	Projected Burgers vector	Perfect Burgers vector
$[0\,0\,1]$	$a[1\,\bar{1}\,0]$	$a[1\,\bar{1}\,0]$
$[\bar{1}\,1\,\bar{1}]$	$1/3a[2\,1\,\bar{1}]$	$a[0\,1\,\bar{1}]$
	$1/3a[\bar{1}\,\bar{2}\,\bar{1}]^a$	$a[\bar{1}\,0\,\bar{1}]^a$
$[\bar{1}\,1\,1]$	$1/3a[1\,2\,\bar{1}]$	$a[1\,0\,\bar{1}]$
	$1/3a[2\,1\,1]$	$a[0\,\bar{1}\,\bar{1}]$

^{a} Not directly observed in our experiments.

into two components: one is perpendicular to the interface and the other is parallel to the interface; while only the latter contributes to the relaxation. Take the $[\bar{1}\,1\,\bar{1}]$ direction and $b = a[0\,1\,\bar{1}]$ MD as an example. The $b = a[0\,1\,\bar{1}]$ can be decomposed according to the following equation:

$$a[0\,1\,\bar{1}] = 1/2a[\bar{1}\,1\,\bar{2}] + 1/2a[1\,1\,0].$$

Here, $1/2a[1\,1\,0]$ is the component perpendicular to the interface, which does not relax the lattice mismatch; instead it has a tilt effect on the NSMO film [19], as will be clarified later. $1/2a[\bar{1}\,1\,\bar{2}]$ is the component parallel to the interface, which mostly relaxes the lattice mismatch. The $1/2a[\bar{1}\,1\,\bar{2}]$ component can be further decomposed as follows:

$$1/2a[\bar{1}\,1\,\bar{2}] = a[0\,0\,\bar{1}] + 1/2a[\bar{1}\,1\,0].$$

In this way, $a[0\,0\,\bar{1}]$ relaxes the lattice mismatch on the (0 0 1) plane, whereas $1/2a[\bar{1}\,1\,0]$ relaxes the lattice mismatch on the $(\bar{1}\,1\,0)$ plane, which means that misfit dislocations with line directions of $\langle 1\,1\,1\rangle$ can relax the misfit strains on both the (0 0 1) and $(\bar{1}\,1\,0)$ planes simultaneously. The decomposition procedure is illustrated in Fig. 6. Next we discuss the misfit relaxation contributed by dislocations with Burgers vectors $[1\,\bar{1}\,0]$ ($b = \langle uvw\rangle$ where $w = 0$) and line direction $[0\,0\,1]$. For the $[0\,0\,1]$ MDs, the explanation is very straightforward. Because their Burgers vectors are parallel to the interface and have no perpendicular component, they also relax the misfit strain effectively.

From the discussion above, it is noted that the misfit relaxation behaviors of these two group dislocations are not independent of each other, but rather are correlated. It seems that the STO (1 1 0) substrate is the factor to induce the unique misfit relaxation behavior. As mentioned earlier, $1/2a[1\,1\,0]$ is the component perpendicular to the interface and does not relax the misfit strain. However, it is found that this component affects the microstructure of the present film. These closely and co-directionally aligned perpendicular components will tilt the NSMO film somewhat away from the STO substrate. Fig. 7 shows direct evidence for the tilt effect of the $[\bar{1}\,1\,\bar{1}]$ MDs. Fig. 7 is a FFT pattern corresponding to Fig. 2. Normally, the diffraction spots 220 from both NSMO and STO should be strictly aligned along the [1 1 0] direction due to the same cubic structure. However, from this pattern, the splitting of the 220 spots of NSMO and STO is clear and gives a tilt angle of NSMO about 2.0° relative to the STO. It should be pointed out that the completely coherent area with no
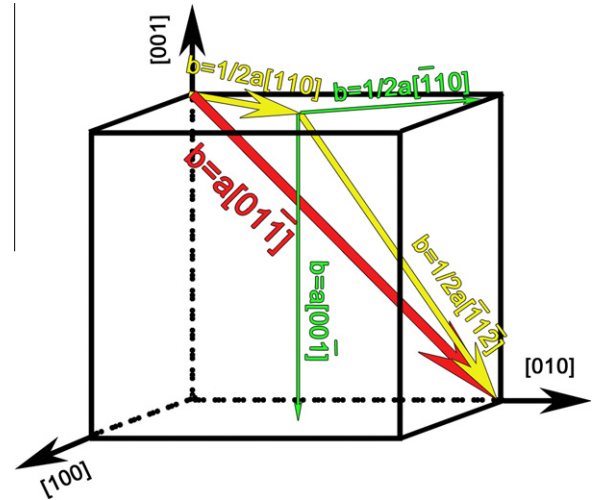

Fig. 6. A schematic diagram showing the Burgers vector decomposition. Big arrow: perfect Burgers vector; middle arrow: out-of-plane component and in-plane component; small arrow: further decomposed in-plane component.

MDs has no such tilt effect. $1\,\bar{1}\,2$ spots for the NSMO and STO are also marked. This situation is very similar to the low-angle boundaries in crystals [22] where the low-angle boundary alignment causes the tilting of both sides of the crystal. A similar observation was found in some Nb/Al$_2$O$_3$ thin-film systems [19]. Actually, the local tilt angle of NSMO film can be calculated based on Frank's formula: $d_{th} = |b|/[2\,\sin(\theta/2)]$ [22]; when the tilt angle θ is small, an approximation can be made:
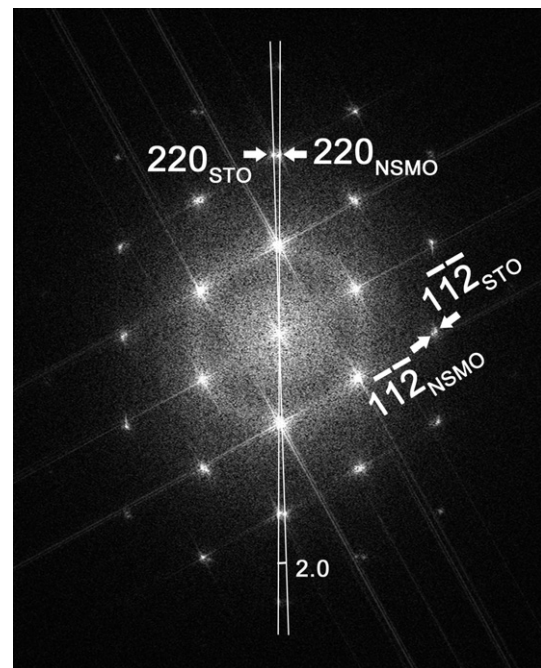
$$\theta \sim b/d_{th},$$

Fig. 7. FFT pattern of Fig. 3. Note that the diffraction spots from the NSMO film are tilted about 2.0° compared with those from the STO substrate.
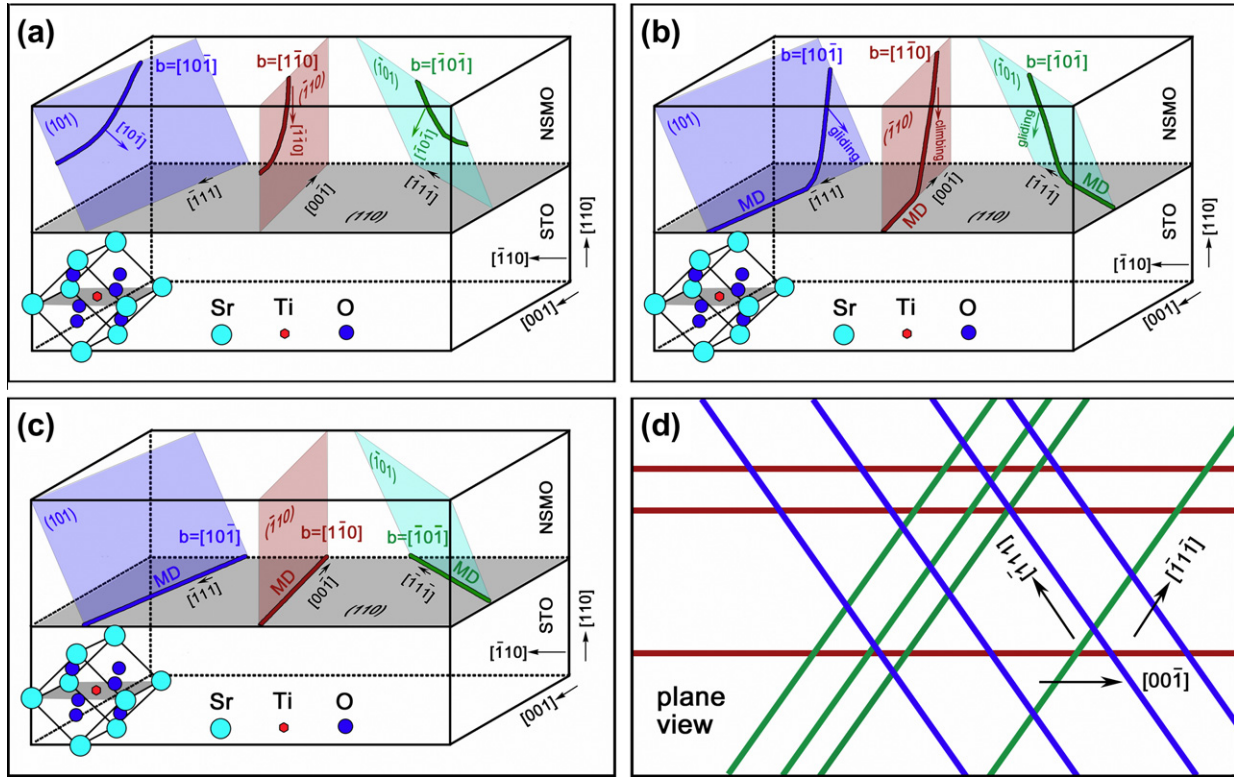
Fig. 8. Schematic diagram illustrating the formation mechanism of the MD in the NSMO/STO (110) system. (a) The initial stage: some dislocation segments lie in the glide planes of $\langle 110 \rangle$. The dislocations with Burgers vectors $a[\bar{1}0\bar{1}]$ and $a[10\bar{1}]$ will move by gliding on their respective glide planes along certain directions while the dislocations with Burgers vectors $a[1\bar{1}0]$ will move up the $(\bar{1}10)$ plane by climbing along the $[\bar{1}\bar{1}0]$ direction. The intersection of the climbing plane and the STO (110) plane is in the $[00\bar{1}]$ direction, whereas the intersections of each of the two slip planes and STO (110) are in the $[\bar{1}1\bar{1}]$ and $[\bar{1}11]$ directions, respectively. (b) The middle stage: as these dislocations move toward the interface, some segments reach the interface and become misfit dislocations while other segments continue to move towards the interface. (c) The final stage: the movement stops and forms a misfit dislocation network at the interface. (d) |A complete misfit dislocation network configuration as seen in plan view, matching well with Fig. 2.

where θ is the tilt angle of NSMO film, b is the magnitude of the MD Burgers vector (perpendicular component of $1/2a[110]$), and d_{th} is the average dislocation space (7 nm in Fig. 3). The calculated tilt angle is then around 2.2°, which is highly consistent with our experiments and implies that in a very local area, the tilt angle of the NSMO film is possibly considerable. The tilting effect makes the strain state more complex in the two-dimensional NSMO film, and consequently may further affect the local Jahn–Teller effect and the phase transition behavior because these properties in manganites are strain sensitive [14].

4.2. The formation mechanisms for the unique MD configuration

For perovskite film systems, MDs could originate from the film by dislocation gliding or climbing and dislocation reaction [17,35]. As a common substrate, the dislocations in STO are surprisingly movable and can glide even below room temperature [36]. Since $\{110\}\langle 110 \rangle$ is a common slip system for STO, which corresponds to $b = a\langle 110 \rangle$-type dislocations [17,36], then gliding or climbing by $a\langle 110 \rangle$-type dislocations in the STO or NSMO to the interface is the most probable way of constructing the $\langle 111 \rangle$ MD configu-

ration, because the intersections of the slip or climb plane and the NSMO/STO (110) interface plane are exactly the $\langle 111 \rangle$ directions. Whether dislocation formation in the present study occurs through gliding or climbing, it is generally believed that gliding is easier. Supposing $a\langle 111 \rangle$ MD can be formed either by gliding or climbing. Dislocations moving by gliding will then have the Burgers vectors $b = 1/3a\langle 112 \rangle$ when viewed from $\langle 111 \rangle$, while dislocations moving by climbing have the Burgers vector $b = a\langle 110 \rangle$. Meanwhile, gliding and climbing will result in different $\langle 111 \rangle$ dislocation lines for a specific $a\langle 110 \rangle$ dislocation. For example, gliding results in a $[\bar{1}1\bar{1}]$ line direction and climbing results in a $[\bar{1}11]$ line direction or vice versa. In comparison with the experiment results above (Figs. 2, 4 and 5), it is deduced that the misfit dislocations with line directions of $\langle 111 \rangle$ are formed through gliding rather than climbing in the present thin-film system. For the $[001]$ MDs, since the slip plane for $b = a[1\bar{1}0]$ is parallel to the interface, climbing will be the only way to reach the interface [16] through thermal activation during high-temperature deposition. Summarizing the dislocation movement behavior, a mechanism is proposed to elaborate the misfit dislocation formation in the present film system. Take $b = a[1\bar{1}0]$ MDs (line direction $[001]$), $a[\bar{1}0\bar{1}]$ and

$a[10\bar{1}]$ MDs (line direction $\langle 111 \rangle$) as an example. Supposing these dislocations come from the NSMO side. In Fig. 8a, at the initial stage, segments of these dislocations near the interface are moving towards the interface driven by the coherency force: $a[1\bar{1}0]$ by climbing on the $(\bar{1}10)$ plane along the $[\bar{1}\bar{1}0]$ direction; $a[\bar{1}0\bar{1}]$ by gliding on the $(\bar{1}01)$ plane along the $[\bar{1}0\bar{1}]$ direction; $a[10\bar{1}]$ by gliding on the (101) plane along the $[10\bar{1}]$ direction. It should noted that the intersections of each of the climb (slip) planes and the (110) plane of STO are in the $[00\bar{1}]$, $[\bar{1}1\bar{1}]$ and $[\bar{1}11]$ directions, respectively. As these dislocations move toward the interface, some segments are pinned by the interface, while other segments are still moving towards the interface, as indicated in Fig. 8b. Finally, the whole $a[1\bar{1}0]$, $a[\bar{1}0\bar{1}]$ and $a[10\bar{1}]$ dislocations are pinned by the interface, forming perfect MDs, as indicated in Fig. 8c and d. Fig. 8d is a schematic pattern showing the complete misfit dislocation network seen in plan view, which agrees well with Fig. 2. For dislocations with a slip plane inclined to the substrate surface, gliding is a reasonable way to form a MD; for dislocations with a slip plane parallel to the substrate surface, climbing is the only way to form a MD if this is possible. In conclusion, it is proposed that the line directions of the MDs are determined by the intersections of the slip plane (climb plane) and the interface plane [19].

It should be emphasized that the discussions above are probably suggestive of general formation mechanisms for $b = a\langle 110 \rangle$-type MDs in perovskite-based film systems, especially the gliding mechanism. For $[001]$-oriented STO substrates, the intersection of some specific $a\langle 110 \rangle$ dislocation slip plane and the interface plane is the $\langle 100 \rangle$ line direction. As a result, an orthogonal MD network forms as observed in Nb-doped $SrTiO_3$ film grown on STO (001) [24]. To further verify this inference for an NSMO crystal with the same composition, 8 nm thick NSMO/STO (001) films were fabricated under the same conditions as the present NSMO/STO (110) film. An orthogonal MD network with line directions of STO $\langle 100 \rangle$ was indeed observed for the 8 nm thick film. The Burgers vectors are determined as $b = a\langle 110 \rangle$.

Moreover, $\langle 111 \rangle$-oriented perovskite substrates have recently attracted much attention due to their potential applications, such as the stabilization of two-dimensional topological insulators [37–39]. We further infer that for the films grown on STO (111) and even other $\langle 111 \rangle$-oriented perovskite substrates, if the MDs have the Burgers vectors $b = a\langle 110 \rangle$-type, the MD lines should run along the $\langle 112 \rangle$ directions because the intersections of the slip planes for some specific $a\langle 110 \rangle$ dislocations and the STO (111) surface plane are the $\langle 112 \rangle$ directions.

5. Conclusion

By means of (S)TEM analysis, the configurations, Burgers vectors and strain relaxation behaviors of MDs in the NSMO/STO (110) film have been investigated with the following findings. A new MD configuration in the NSMO/STO (110) film is identified and analyzed. It is found that two types of misfit dislocations contribute to the misfit strain relaxation. One has the Burgers vectors $a\langle 011 \rangle (w \neq 0)$ with line directions of STO $\langle 111 \rangle$; the other has the Burgers vectors $a[1\bar{1}0] (w = 0)$ and line direction of STO $[001]$. The $\langle 111 \rangle$ MDs relax both the (001) and $(\bar{1}10)$ plane lattice mismatch simultaneously, while the $[001]$ MDs only relax the $(\bar{1}10)$ plane lattice mismatch. Moreover, the perpendicular components of the $\langle 111 \rangle$ MDs have a tilt effect on the NSMO film. It is proposed that the MDs were formed by gliding and climbing and finally pinned by the NSMO/STO (110) interface, constructing a special MD configuration. The line directions of the MDs are determined by the intersections of the slip plane (climb plane) and the interface plane. Having elucidated the formation mechanism, it is now possible to draw inferences about the possible $a\langle 110 \rangle$-type MD configuration of a film on STO (111). These MDs should have $\langle 112 \rangle$-type line directions. These findings may provide some insight for understanding the anisotropic elastic strain relaxation features of $Nd_{1-x}Sr_xMnO_3$ films grown on STO (110).

References

[1] von Helmolt R, Weeker J, Holzapfel B, Schultz L, Samwer K. Phys Rev Lett 1993;71:2331.
[2] Lai KJ, Nakamura M, Kundhikanjana W, Kawasaki M, et al. Science 2010;329:190.
[3] Kajimoto R, Yoshizawa H, Kawano H, Kuwahara H, Tokura Y. Phys Rev B 1999;60:9506.
[4] Kuwahara H, Tomioka Y, Asamitsu A, Moritomo Y, Tokura Y. Science 1995;270:961.
[5] Maezono R, Ishihara S, Nagaosa N. Phys Rev B 1998;58:11583.
[6] Aliev AM, Batdalov AB, Gamzatov AG. Low Temp Phys 2010;36:171.
[7] Xu SH, Moritomo Y, Machida A, Ohoyama K, Kato K, Nakamura A. Phys Rev B 2002;66:024420.
[8] Zhang Q, Zhang YQ, Zhu YL, Cho JH, Zhang ZD. Phys Status Solidi A 2010;207:2558.
[9] Kawano H, Kajimoto R, Yoshizawa H, Tomioka Y, Kuwahara H, Tokura Y. Phys Rev Lett 1997;78:4253.
[10] Yoshizawa H, Kawano H, Fernandez-Baca JA, Kuwahara H. Phys Rev B 1998;58:R571.
[11] Zhang YQ, Meng H, Wang XW, Wang X, Guo HH, Zhu YL, et al. Appl Phys Lett 2010;97:172502.
[12] Estradé S, Rebled JM, Arbiol J, Peiró F, Infante IC, Herranz G. Appl Phys Lett 2009;95:072507.
[13] Qin YL, Zandbergen HW, Yang ZQ. Aarts J Philos Mag 2005;85:4465.
[14] Ogimoto Y, Nakamura M, Takubo N, Tamaru H, Izumi M, Miyano K. Phys Rev B 2005;71:060403 (R).
[15] Uozu Y, Wakabayashi Y, Ogimoto Y, Takubo N, Tamaru H, Nagaosa N, et al. Phys Rev Lett 2006;97:037202.
[16] Langjahr PA, Lange FF, Wagner T, Rühle M. Acta Mater 1998;46:773.

[17] Suzukia T, Nishia Y, Fujimotoa M, et al. Philos Mag A 1999;79:2461.

[18] Matthews JW. In: Nabarro FRN, editor. Dislocations in solids, vol. 2. Amsterdam: North-Holland; 1979. p. 461.

[19] Gutekunst G, Mayer J, Vitek V, Rühle M. Philos Mag A 1997;75:1357.

[20] Sigle W, Sarbu C, Brunner D, Rühle M. Philos Mag 2006;86:4809.

[21] Wang ZC, Karato SI, Fujino K. Phys Earth Planet In 1993;79:299.

[22] Zhang ZL, Sigle W, Rühle M. Phys Rev B 2002;66:094108.

[23] Zhang ZL, Sigle W, Kurtz W, Rühle M. Phys Rev B 2002;66:214112.

[24] Zhu YL, Ma XL, Li DX, Lu HB, et al. Acta Mater 2005;53:1277.

[25] Lu CJ. Appl Phys Lett 2004;85:2768.

[26] Birajdar BI, Chopra A, Alexe M, Hesse D. Acta Mater 2011;59:4030.

[27] Nakamura M, Ogimoto Y, Tamaru H, et al. Appl Phys Lett 2005;86:182504.

[28] Kasai M, Kuwahara H, Moritomo Y, Tomioka Y, Tokura Y. Jpn J Appl Phys 1996;35(Part 2):L489.

[29] Wakabayashi Y, Bizen D, Nakao H, Murakami Y, Nakamura M, Ogimoto Y, et al. Phys Rev Lett 2006;96:017202.

[30] Wang X, Zhu YL, He M, Lu HB, Ma XL. Acta Mater 2011;59:1644.

[31] Zhu YL, Wang X, Zhuo MJ, Zhang YQ, Ma XL. Philos Mag Lett 2010;90:323.

[32] Zhu YL, Zheng SJ, Ma XL, Feigl L, Alexe M, Hesse D, et al. Philos Mag 2010;90:1359.

[33] Jia CL, Mi SB, Urban K, Vrejoiu I, Alexe M, Hesse D. Phys Rev Lett 2009;102:117601.

[34] Qi XY, Miao J, Duan XF, Zhao BR. J Cryst Growth 2005;277:218.

[35] Sun HP, Pan XQ, Haeni JH, Schlom DG. Appl Phys Lett 2004;85:1967.

[36] Gumbsch P, Taeri-Baghbadrani S, Brunner D, Sigle W, Rühle M. Phys Rev Lett 2001;87:085505.

[37] Rüegg A, Fiete GA. Phys Rev B 2011;84:201103 (R).

[38] Yang KY, Zhu WG, Xiao D, Okamoto S, Wang ZQ, Ran Y. Phys Rev B 2011;84:201104 (R).

[39] Chakhalian J, Millis AJ, Rondinelli J. Nat Mater 2012;11:92.